A hydrodynamic basis for off-axis Brownian diffusion under intermediate confinements in micro-channels

International Journal of Multiphase Flow 143 (2021) 103772

Contents lists available at ScienceDirect

International Journal of Multiphase Flow

journal homepage: www.elsevier.com/locate/ijmulflow

A hydrodynamic basis for off-axis Brownian diffusion under intermediate confinements in micro-channels

Ananda Subramani Kannan [a,*], Andreas Mark [b], Dario Maggiolo [a], Gaetano Sardina [a], Srdjan Sasic [a], Henrik Ström [a]

[a] Department of Mechanics and Maritime Sciences, Division of Fluid Dynamics, Chalmers University of Technology, Göteborg, 412 96, Sweden
[b] Fraunhofer-Chalmers Research Centre, Göteborg, 412 88, Sweden

ARTICLE INFO

Keywords:
Brownian diffusion
CFD
Hindered diffusion
Hydrodynamic resistance
Immersed boundary method
Micro-channel and mobility

ABSTRACT

The mobility of a Brownian particle diffusing in a micro-channel is heterogeneous and spatially dependent on the surrounding hydrodynamic resistance fields. The positional asymmetry of such a diffusing particle leads to anisotropies in the observed diffusive behavior. In this paper, we probe such directionally varying diffusive behavior of a spherical nanoparticle diffusing at a location off-set from the centerline of a square micro-channel in a quiescent fluid. This investigation is carried out over varying degrees of intermediate hydrodynamic confinements. A coupled Langevin-immersed boundary method is used for these assessments. We observe that the co-axial diffusivity may be slightly enhanced during off-axis hindered diffusion when compared with a corresponding centerline diffusive behavior. We attribute this increased particle diffusivity to a reduced co-axial fluid resistance through a hydrodynamic basis derived using steady-state CFD solutions to the corresponding Stokes problem. For co-axial motion, the particle creates a recirculating flow pattern around itself when moving along the centerline, whereas it drags along the fluid in between itself and the wall when in close proximity to the latter. These contrasting flow behaviors are responsible for the unexpected enhancement of the co-axial diffusivity for some off-axis positions under intermediate hydrodynamic confinements.

1. Introduction

The diffusion of Brownian particles in confined environments is a well-explored problem (Happel and Brenner, 1983). An in-depth understanding of the hindered transport of such nanoparticles can aid in developing novel nanoengineering-based concepts for a wide range of applications. Some typical examples include designing filters for the entrapment of particulate matter (Kannan et al., 2019), evaluating the performance of nano-electrofuels in redox flow batteries (Sokolov et al., 2016), bio-engineering applications involving transport of magnetized nano-particles in lab-on-a-chip devices (Derks et al., 2008), surface-based biosensors (Squires et al., 2008) and targeted drug delivery using functionalized nanocarriers (Ayyaswamy et al., 2013). In optimizing these applications, the ability to predict the behavior of individual nanoparticles in confined environments is of utmost importance. Such predictions are challenging as the non-equilibrium thermal fluctuations in the system render the relationship between the characteristics of the particle (and its surrounding environment) and its observable behavior stochastic. These challenges are further aggravated by the fact that under tight confinements, the hydrodynamic effect on the particle from the surrounding fluid changes nature — it is no longer a monotonous function of the particle–wall distance as the balance between parallel and normal hydrodynamic resistances is shifted (Kannan et al., 2021).

It is well established that the mobility (defined as the ratio of the particle terminal velocity to the hydrodynamic frictional force) of a Brownian particle in a confined system is reduced in relation to the free (or unbounded) diffusion case (MacKay and Mason, 1961; Bevan and Prieve, 2000; Dufresne et al., 2000; Choi et al., 2007; Gentile et al., 2015; Mo and Raizen, 2019). This effect is due to the increased drag from the alteration of the hydrodynamic interaction between the particle and the fluid due to external boundaries (Brenner, 1961). Correspondingly, the mobility and (consequently) diffusivity of the particle are functions of the position of the Brownian particle in relation to the boundary walls, implying that the mobility is heterogeneous and spatially dependent (Skaug et al., 2015). It follows that these quantities can be corrected by a factor λ (also termed as the reduction in mobility), which represents the extent of the deviation from the analytical unbounded behavior (Brenner, 1961; Happel and Brenner, 1983; Bevan and Prieve, 2000; Dufresne et al., 2000; Kihm et al., 2004; Choi et al., 2007), in order to accurately represent hindered diffusion.

* Corresponding author.
E-mail address: ananda@chalmers.se (A.S. Kannan).

https://doi.org/10.1016/j.ijmultiphaseflow.2021.103772
Received 29 December 2020; Received in revised form 11 May 2021; Accepted 2 August 2021
Available online 9 August 2021

For a more detailed account of related hindered diffusion theories, the reader is referred to the reviews by Deen (1987), Burada et al. (2009), Radhakrishnan et al. (2019) and Mo and Raizen (2019) and to the classical books by Happel and Brenner (1983) and Kim and Karrila (1991).

Correspondingly, for a particle that is small in relation to the bounding geometry, well-established rules of thumb indicate that the hydrodynamic resistance to motion increases as the particle is positioned closer to the wall and that this effect is larger for wall-normal motion than for parallel motion. However, it is noticeable in the mobility data of Gubbiotti et al. (2019) that as the confinement increases, the hydrodynamic effect for parallel motion will eventually surpass wall-normal motion in the central region of a small duct, as the minimum in the hydrodynamic influence on the wall-parallel particle motion shifts from the centerline to an off-axis position. In a recent paper Kannan et al. (2021), we identified a similar bias in the hydrodynamic resistances along the co-axial and wall-normal directions on a Brownian particle diffusing in a square micro-channel. We noted that the former was greater than the latter for a particle diffusing co-axially along the centerline of the micro-channel. Such effects have not yet been fully understood or characterized previously. Consequently, in this work, we analyze the impact of such tight confinements on the Brownian motion of a spherical particle by further extending the range of confinements and by focusing on the pure hydrodynamic effect of confinement (without the action of any external field). Fully understanding this hydrodynamic bias is relevant when assessing Brownian transport in micro-channels with nanoparticles that are not negligible in size when compared with the channel width.

The existing body of work in this field mainly extends the hydrodynamic theories of Brenner and others (Brenner, 1961; Happel and Brenner, 1983; Felderhof, 2005; Michaelides, 2016) for a spherical Brownian particle moving co-axially in a cylindrical channel towards off-axis diffusion. Mavrovouniotis and Brenner (1988) achieved this by including an extra dispersion contribution (due to the positional asymmetry) in addition to the direct hindered-diffusion effect of the tube walls upon the mean co-axial diffusivity. Further, Dechadilok and Deen (2006) presented an improved correlation based on the off-axis hydrodynamic results of Higdon and Muldowney (1995) and Mavrovouniotis and Brenner (1988). A hydrodynamic basis cannot be derived from the expressions presented in that work (Dechadilok and Deen, 2006) since all directional information is contained within a single scalar expression for λ, whereas λ is a function of both the position and direction of motion of the particle. More recently, Uma et al. (2011) used an iterative fluctuating hydrodynamics (FH) approach to estimate the dependence of the co-axial and wall-normal estimates of λ as a function of the distance from the walls of a circular vessel in a quiescent medium. Gubbiotti et al. (2019) used the dissipative particle dynamics (DPD) framework (a kinetic-theory-based approach) to construct a spatial mobility field for a Brownian particle diffusing in a cylindrical channel.

While these recent efforts have in principle probed the anisotropy in the hydrodynamic resistances, similar studies on hindered diffusion in arbitrary geometries and under asymmetric conditions are scarce. Moreover, the origin of the anisotropy in the hydrodynamic resistances felt by a Brownian particle under confinement has not been adequately probed. Thus, with this paper we aim at providing fresh insights into such systems. We present the relevant hydrodynamic basis for off-axis hindered diffusion in a square micro-channel under intermediate confinement (i.e. the particle size is non-negligible in relation to the channel size while still smaller than the hydraulic diameter) for small Reynolds numbers. We use a previously developed and validated multiphase direct numerical simulation (DNS) technique, a Langevin-immersed Boundary method or *LaIBM* (Kannan et al., 2019, 2021), to probe the relevant hydrodynamic fields around the Brownian particle. We evaluate the hindered diffusion initiated along the centerline (co-axial) of the channel as well as at a location that is off-set from this centerline (midway between the center and walls), under different confinements or blockage ratios (B given as a/d_p, where a is the side of the square duct and d_p the diameter of the spherical particle). The obtained results are compared with continuum-resolved (steady-state) simulations for the single particle hydrodynamics using a settling particle in a channel. This is done in order to establish the necessary hydrodynamic basis for the observed hindered diffusion phenomena at high resolutions.

2. Methodology

We combine two separate computational frameworks for the current analysis: *LaIBM* (for the hindered Brownian diffusion simulations) and steady-state *CFD* simulations (for in-depth analysis of the hydrodynamic fields). This is done in order to establish the relevant hydrodynamic basis for hindered diffusion. These are both introduced in the following.

2.1. Langevin-immersed boundary method (LaIBM)

The *LaIBM* framework handles the particle in the Lagrangian frame of reference and the fluid in the Eulerian one, respectively. The immersed boundary method (IBM) (Peskin, 1982; Mittal and Iaccarino, 2005) is used to couple these descriptions. In this method, the Navier–Stokes equations are discretized on a Cartesian grid and the presence of the particle is modeled using boundary conditions or source terms. Furthermore, *LaIBM* utilizes a dynamic octree grid for the necessary refinements (around the IB) and a second-order accurate mirroring immersed boundary method (Mark and van Wachem, 2008; Mark et al., 2011; Kannan et al., 2019, 2021) to implicitly impose the necessary no-slip boundary condition at the IB surface. This unique and stable second-order accurate implicitly formulated immersed-boundary condition (IBC) is central to the efficiency and accuracy of this framework.

The Eulerian (or continuum) description of the fluid around the immersed particle is given by the Navier–Stokes equations:

$$\rho_f \left(\frac{\partial \boldsymbol{v}}{\partial t} + \boldsymbol{v} \cdot \boldsymbol{\nabla} \boldsymbol{v} \right) = -\boldsymbol{\nabla} P + \mu_f \boldsymbol{\nabla}^2 \boldsymbol{v} + f_i,$$
$$\boldsymbol{\nabla} \cdot \boldsymbol{v} = 0, \tag{1}$$

where, ρ_f, μ_f, $\boldsymbol{v}$ and P represent the fluid density, dynamic viscosity, velocity and pressure, respectively. The term f_i represents any external source term. This set of equations is solved together with an implicit Dirichlet IB condition. A more detailed description of the method is available in Mark and van Wachem (2008), Mark et al. (2011). The fluid force acting on the IB, $\mathbf{F_{IB}}$, is calculated by integrating the fluid stresses over the surface of the IB as:

$$\mathbf{F_{IB}} = \int_{IB} \bar{\bar{\sigma}} \cdot \mathbf{n} dS = \int_{IB} \left[-P\mathbf{n} + \bar{\bar{\tau}} \cdot \mathbf{n} \right] dS$$
$$= \int_{IB} \left[-P\mathbf{n} + \left(\mu_f \{ \boldsymbol{\nabla} \boldsymbol{v} + (\boldsymbol{\nabla} \boldsymbol{v})^T \} \right) \cdot \mathbf{n} \right] dS, \tag{2}$$

where $\bar{\bar{\sigma}}$ is the total fluid stress tensor, $\bar{\bar{\tau}}$ the shear stress tensor, and S denotes a surface with normal $\mathbf{n}$. The corresponding torque, $\mathbf{T_{IB}}$, on the IB with a position vector $\mathbf{r}$ is calculated using:

$$\mathbf{T_{IB}} = \int_{IB} \mathbf{r} \times \boldsymbol{\sigma} \cdot \mathbf{n} dS. \tag{3}$$

The particulate phase in the *LaIBM* framework is governed by the Lagrangian Langevin equation of motion (Langevin, 1908; Uhlenbeck and Ornstein, 1930; Chandrasekhar, 1943; Ounis and Ahmadi, 1990b; Li and Ahmadi, 1992). This equation balances the macro-scale hydrodynamic drag on the particle with the molecular-scale Brownian fluctuations. For the hindered diffusion of a particle with mass m_p, translational velocity $\mathbf{u_p}$, angular velocity $\boldsymbol{\omega_p}$ and moment of inertia $\boldsymbol{J}$, the corresponding Langevin equation is described as:

$$m_p \frac{\mathrm{d}\mathbf{u_p}}{\mathrm{d}t} = \mathbf{F_{IB}} + \mathbf{F_{Brownian}}, \tag{4}$$

$$\mathbf{J}\frac{\mathrm{d}\boldsymbol{\omega}_p}{\mathrm{d}t} = \mathbf{T_{IB}} - \boldsymbol{\omega}_p \times \mathbf{J}\cdot\boldsymbol{\omega}_p. \tag{5}$$

In Eqs. (4) and (5), note that the continuum resolved translational ($\mathbf{F_{IB}}$) and rotational ($\mathbf{T_{IB}}$) hydrodynamic fields are directly used in the Langevin equation, enforcing a direct coupling of the Eulerian solution with the corresponding Langevin equation of motion. In the presence of walls and/or other particles, the friction coefficient ($\gamma_{IB} = \mathbf{F_{IB}}/\mathbf{u_p}$) becomes spatially dependent, which is thus inherently captured by the current framework. We also note that accounting for the particle inertia and integrating the particle equation of motion using a mid-point rule algorithm (Newmark, 1959; Kannan et al., 2021) invalidates the need for adding an artificial drift velocity to the Langevin equation, as may otherwise be needed for position-dependent friction (Grassia et al., 1995; Farago and Grønbech-Jensen, 2014).

The directional reduction in mobility, λ, is required in the stochastic forcing term $\mathbf{F_{Brownian}}$, and it is here estimated *on-the-fly* by normalizing the magnitude of the hydrodynamic force on the confined Brownian particle ($\mathbf{F_{IB}}$) with the corresponding Stokes drag on the same particle when diffusing in an unbounded domain. This is given as:

$$\lambda_i = \frac{\|\mathrm{F_{IB,1}}\|}{\gamma\|\mathrm{u_{p,i}}\|}. \tag{6}$$

Here, the Stokes friction factor γ is defined for a fluid with the dynamic viscosity μ_f as $\gamma = 3\pi\mu_f d_p$, and d_p is the particle diameter. The particle response time in the unbounded limit, τ_p, is used as the characteristic time scale, and it is given as:

$$\tau_p = m_p/\gamma. \tag{7}$$

The force $\mathbf{F_{Brownian}}$ represents the Brownian fluctuations in the particle motion. In the case of a position-dependent friction (or, equivalently, position-dependent diffusion coefficient) as in the current work, this multiplicative noise term becomes a product of a state-dependent prefactor proportional to the square root of the diffusion coefficient and a state-independent Gaussian white noise function (Lau and Lubensky, 2007). We thus model this force as (Uhlenbeck and Ornstein, 1930; Ounis and Ahmadi, 1990a,b; Li and Ahmadi, 1992):

$$\mathrm{F_{Brownian,i}}(t) = \mathrm{G}_i\sqrt{\frac{2\gamma\lambda_i k_B T}{\Delta t}}. \tag{8}$$

Here, $\mathbf{G}$ is a vector of normally distributed independent random numbers of zero mean and unit variance (Gaussian distribution), Δt is the duration during which the Brownian force is active, k_B is the Boltzmann constant, and T is the absolute temperature. This Brownian force produces a diffusive behavior characterized by the spatially dependent Brownian diffusivity D_i, which is a function of the system configuration and reflects the total hydrodynamic interactions as perceived by the particle in the current location at the current time:

$$D_i = \frac{D_\infty}{\lambda_i} = \frac{k_B T}{\gamma\lambda_i}, \tag{9}$$

where $D_\infty = k_B T/\gamma$ is the Stokes–Einstein (bulk) diffusivity (Brenner, 1982; Mavrovouniotis and Brenner, 1988; Dechadilok and Deen, 2006).

The linear and angular momentum conservation equations (Eqs. (4) and (5)) are integrated using the Newmark time-marching scheme with the constant average acceleration method (mid-point rule approach) (Newmark, 1959) and a time step $\delta t < \Delta t < \tau_p$. It is reasonable to assume that changes to the system configuration are small on the time scale τ_p in typical hindered diffusion problems (Batchelor, 1976). The use of a small time step δt ensures a small displacement and thus a close correspondence between the spatial and temporal averages of the friction coefficient along the interval that the particle passes, which in turn ensures convergence of the integration irrespective of the interpretation of the stochastic integral (Lau and Lubensky, 2007). We note however that the employed scheme is compliant with the Itô interpretation (Itô, 1973). The time step δt is also used in the integration of Eq. (1).

In conclusion, the variation in the mean-squared displacement, MSD_i, of the particle over sufficiently long times ($t \gg \tau_p$) should reproduce the spatially-dependent diffusivity, given as:

$$MSD_i = \frac{1}{N}\sum_{n=1}^{N}\left[\mathrm{x_{p,i,n}}(t+dt) - \mathrm{x_{p,i,n}}(t)\right]^2 = 2D_i t, \tag{10}$$

along the ith direction, where $\mathrm{x_{p,i,n}}$ is the particle position in the nth observation among a total of N observations, and dt is a time interval (to be specified in Section 4). This result is dependent on the condition that the total hydrodynamic force on the particle can be obtained from the resolved force $F_{IB,i}$ with the current hydrodynamic interaction effect obtained from Eq. (6) (Kannan et al., 2021). We use an in-house multiphase flow solver `IPS IBOFlow`, that utilizes the mirroring immersed-boundary method to handle the moving particles efficiently (Rundqvist et al., 2010; Göhl et al., 2018; Göhl et al., 2018; Mark et al., 2013; Johnson et al., 2015; Wettervik et al., 2015; Ingelsten et al., 2019, 2020). An overview of the *LaIBM* framework is shown in Fig. 1. For more details on the framework, as well as a thorough validation, the reader is referred to our previous works (Kannan et al., 2019, 2021).

2.2. Steady-state computational fluid dynamics (CFD)

In addition to the continuum-based multiphase DNS framework *LaIBM*, we also use a conventional steady-state computational fluid dynamics *(CFD)* framework to establish a hydrodynamic basis for the results presented in this paper. This framework is chosen so as to off-set the computational requirements of the proposed DNS method, thereby permitting a wider configuration space. Consequently, the steady-state Navier–Stokes equations are discretized within a finite-volume framework (Versteeg and Malalasekera, 1995) and solved using the pseudo-transient pressure-based solver available in `ANSYS Fluent 2019 R3`, with second-order accurate spatial discretization schemes used for all involved terms.

$$\rho_f(\boldsymbol{v}\cdot\boldsymbol{\nabla}\boldsymbol{v}) = -\boldsymbol{\nabla}P + \mu_f\boldsymbol{\nabla}^2\boldsymbol{v},$$
$$\boldsymbol{\nabla}\cdot\boldsymbol{v} = 0. \tag{11}$$

The particulate phase is defined as a fixed volume wherein the desired velocity is prescribed. The resulting hydrodynamic fields around this boundary region are utilized to extract the necessary hydrodynamic bases.

3. Numerical setup

The particle–fluid system studied in this paper is specified in Table 1. The hydrodynamic confinements are represented in terms of a blockage ratio, B, given as a/d_p (where a and d_p are the channel width and particle diameter, respectively). The assessments are carried out using a single spherical Brownian nanoparticle with a diameter of 400 nm. Further, the longitudinal extent of all the domains used in the diffusion simulations of this study is $20d_p$, with periodic conditions imposed along this direction. This length is chosen to minimize any inlet/outlet effects due to the applied boundary conditions on the particle motion. The corresponding domain, along with the axis of orientation (x is the co-axial direction while y and z are the wall-normal directions), is shown in Fig. 2. The locations of the particle in relation to the z-height of the micro-channel are also indicated in this figure with the off-axis diffusion carried out at a location midway between the centerline and the wall. These simulations are done at a low particle Reynolds number ($Re_p = d_p V^\infty_{rms}\rho_f/\mu_f = 3\cdot10^{-3}$, where the root mean square velocity $V^\infty_{rms} = \sqrt{k_B T/m_p} = 1\cdot10^{-4}$ m/s is for an equivalent unbounded Brownian motion of a 400 nm particle) and at a particle–fluid density ratio of 1000, with k_B and T the Boltzmann constant and temperature of the fluid, respectively. These choices are made to maintain the validity of the current form of the

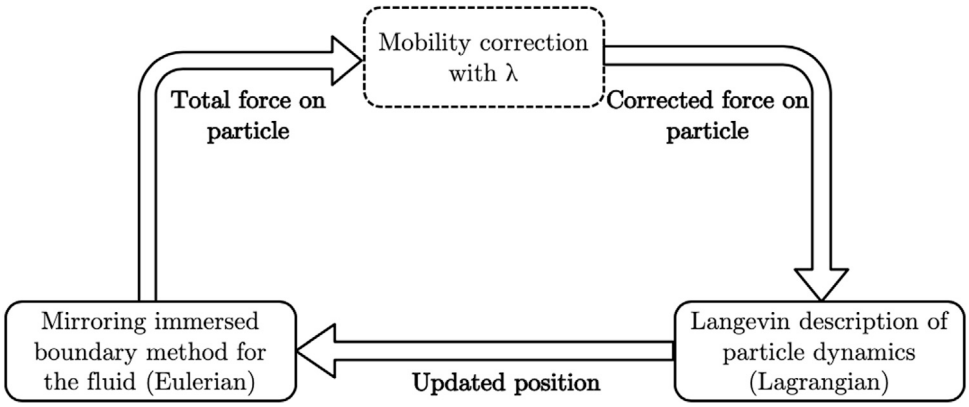

Fig. 1. Overview of the *LaIBM* framework: the particle dynamics are handled on a Lagrangian basis while the surrounding fluid is resolved in an Eulerian framework. Note that the Lagrangian basis utilizes the resolved fluid stresses on the particle (from the Eulerian solution) to compute/correct the particle mobility. This framework is two-way coupled.

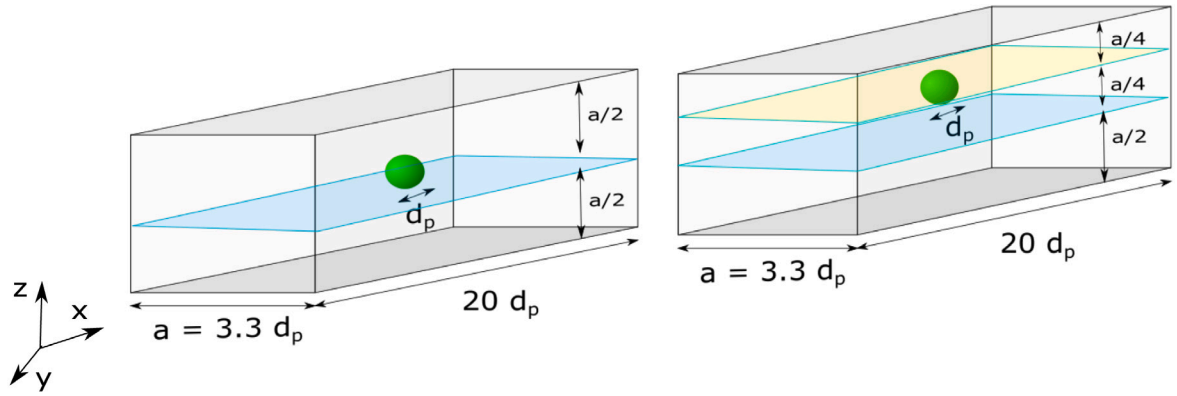

Fig. 2. Examples of the simulation domain: diffusion in the vicinity of the centerline (at $a/2$) inside a straight square micro-channel (**left panel**) and diffusion originating from an off-axis position (at $a/4$) inside a straight square micro-channel (**right panel**). The dimensions are in terms of the particle diameter (d_p). Note that x is the co-axial direction, while z is the wall-normal direction under study here. The corresponding x–y planes at different z positions are depicted in the square micro-channel schematics.

Table 1
Simulation details for the hindered diffusion cases (both centerline and off-axis).

Domain details[+]	Square micro-channel
Size (in d_p)	$a, h = 4.6$, $l = 20$ $a, h = 3.3$, $l = 20$ $a, h = 2.3$, $l = 20$
Simulation details	
Spatial resolution, in *cells*/d_p	96
Temporal resolution δt, in τ_p	1/200
Total duration T, in τ_p^*	100

[+] l is the length, a is the width and h is the height.

Langevin equation (i.e. in Eq. (4) — unsteady effects such as history and added mass forces are negligible). In the simulation setup presented (in Table 1) we use the particle response time τ_p (see Eq. (7)) and the particle diameter d_p for non-dimensionalizing the temporal and spatial details, respectively. Further, since we deal with nanoparticle motion, gravitational acceleration is deemed negligible. These simulations are carried out under varying degrees of hydrodynamic confinement, to gauge the impact of particle blockage in the channel.

We use steady-state continuum computational fluid dynamics simulations of a constant-velocity spherical particle in a square micro-channel to establish a hydrodynamic basis for the hindered diffusion studies. In these studies, we investigate several different locations along the z-height of the channel for the spherical particle, from the centerline to a z-location close to the wall. Furthermore, we run simulations at blockage ratios (B) 4.6, 3.3 and 2.3, in order to span the requisite degree of intermediate confinements needed to establish a relevant hydrodynamic basis. The Reynolds number (based on the hydrodynamic radius of the duct) is maintained at $1{\cdot}10^{-3}$ (Stokes flow). Mesh convergence is obtained by successively refining a base mesh in regions of large gradients of velocity and pressure, until the total force on the spherical particle does not change more than a factor 10^{-3} with further refinements. The base mesh uses a resolution of 1/10th of the particle radius in the region occupied by the particle and 1/20th of the duct radius in the far-field, which yields approximately 650,000 cells. The total number of cells after refinement varied with the geometrical configuration, but was within the range 1.5–5 million. The length of the cylindrical duct is 20 times its hydrodynamic radius, with the particle positioned in the middle along this co-axial coordinate direction. No-slip boundary conditions are enforced along the duct walls and free-slip conditions at the far-field ends. Note that since the Stokes problem is being solved, the corresponding convective contributions in Eq. (11) are negligible.

4. Validation of the numerical methods

The performance of the *LaIBM* framework has been thoroughly validated in our earlier work (Kannan et al., 2019, 2021). Correspondingly, the simulations are carried out at these predetermined spatial and temporal resolutions. Further, the Brownian forcing (see Eq. (8)) is updated in intervals of $\Delta t = \tau_p/10$ to allow for an adequate resolution of the particle acceleration. We have used a pure one-way coupled Langevin point-particle unbounded diffusion case to establish the minimum criteria in terms of simulation duration and time-averaging interval. Other details on the statistical variability in the

Table 2
Validation of the steady-state *CFD* methodology against the analytical solution of Haberman and Sayre (1958), λ_{HS1958}, for co-axial motion of a particle along the centerline of a cylindrical duct. Also listed are comparisons with the DPD results of Gubbiotti et al. (2019), λ_{G2019}.

Blockage ratio	λ_{HS1958}	λ_{CFD}	λ_{G2019}
20.00	1.12	1.12	
4.87	1.71	1.70	1.63
4.00	1.98	1.96	
2.87	2.87	2.86	2.68
2.00	5.87	5.84	

Table 3
Non-dimensional location X^*, which corresponds to the off-axis position $a/4$ in Fig. 2b, at which the $LaIBM$ assessments are carried out (for each chosen blockage ratio).

Blockage ratio	X^*
4.60	0.638
3.30	0.717
2.30	0.882

modeled stochastic process are available in our previous work (Kannan et al., 2019, 2021). The final criteria chosen (based on this prior work) are a total simulation duration (T) of $100\tau_p$ and an interval of $5\tau_p$ for the *MSD* calculations. These simulation settings are further listed in Table 1.

The steady state *CFD* framework is validated by comparing its performance for cylindrical ducts to the analytical results of Haberman and Sayre (1958). This analytical result is given (in terms of B) as:

$$\lambda_{HS1958} = \frac{\left(1 - 0.75857B^{-5}\right)}{\left(1 - 2.1050B^{-1} + 2.0865B^{-3} - 1.7068B^{-5} + 0.72603B^{-6}\right)}. \tag{12}$$

The reduction in particle mobility due to hydrodynamic confinement is deduced from the *CFD* results as:

$$\lambda^i_{CFD} = \frac{F^i}{F^i_{Stokes}}, \tag{13}$$

where F^i and F^i_{Stokes} are the total drag forces on the particle along the ith direction under confinement and when unbounded, respectively. We have confirmed that we are able to reproduce the analytical results of Haberman and Sayre (1958) (Eq. (12)) within $\pm 1\%$ in a cylindrical duct with this approach for B ranging from 20 to 2. These results are presented in Table 2. Furthermore, the DPD results of Gubbiotti et al. (2019) are also listed in this table to demonstrate the accuracy attained in the steady-state *CFD* framework.

5. Results and discussion

In this paper we assess the off-axis hindered diffusion behavior of a spherical nanoparticle diffusing under intermediate confinements in a square micro-channel. These assessments are undertaken to characterize and probe the relevant hydrodynamic behavior of such Brownian particles. Furthermore, a hydrodynamic basis is derived using steady-state *CFD* simulations in order to support the observed trends. These results are elaborated in the following.

5.1. Off-axis hindered diffusion under intermediate confinements

The diffusion of a Brownian particle at a location off-set from the centerline of a square micro-channel is assessed under the conditions specified in Table 1. These assessments are carried out at a non-dimensional location (along the z-axis) given as:

$$X^* = \frac{2p^z - a}{a - d_p}, \tag{14}$$

where, p^z is the location (along the wall-normal z-direction) of the particle between the center of the channel and the walls (i.e. at $X^* = 0$ the particle is located on the centerline, while at $X^* = 1$ the particle touches the wall). Note that the non-dimensional locations listed in Table 3 correspond with the initial off-axis position midway between the centerline and the wall as shown in Fig. 2b.

Fig. 3 summarizes the off-axis hindered diffusion assessments done, showing both the particle drift/displacements (in the top panel) and the resulting directional mean-squared-displacements (MSD^i) that are calculated using Eq. (10) (bottom panel). We represent the drift of the particle in terms of a non-dimensional displacement (along the ith direction from the particle origin) as:

$$P^{i*} = p^{i*} - p^{i*}_{origin}, \tag{15}$$

where, p^{i*} is the non-dimensional particle location given as $p^{i*} = p^i/d_p$. The mean-squared displacements are non-dimensionalized by the diffusional length scale for unbounded diffusion as:

$$MSD^{i*} = \frac{MSD^i}{D^\infty \tau_p^\infty}, \tag{16}$$

where, τ_p^∞ is the response time of an unbounded Brownian particle. Note that the wall-normal motion is represented by the z-coordinate as the particle is off-set along this direction (y-symmetric).

Under these intermediate confinements, there is a noticeable difference in the mean drift of the Brownian particle across different blockage ratios as well as for the centerline and off-axis positions. The displacement of a freely diffusing Brownian particle ($\lambda = 1$) is also shown in Fig. 3 to appreciate the overall effect from the confinement. It is evident that the Brownian particle under confinement is displaced lesser than a corresponding unbounded particle. This is expected since the confinement increases the hydrodynamic resistance on the Brownian particle leading to its net lower drift (owing to the enhanced particle drag). There is, however, an interesting trend noticeable when comparing diffusion along the centerline with the corresponding off-axis cases listed in Table 3 (at $a/4$), under such intermediate confinements. In the co-axial direction, we can notice that a Brownian particle diffusing in the off-axis region is displaced more than the corresponding centerline case. Along the wall-normal direction, however, the opposite trend is observed with the Brownian particle in the off-axis cases being displaced significantly lesser than their corresponding centerline counterparts. These trends are also reflected in the reported MSD^{i*}.

We further summarize these anisotropic trends in terms of the respective directional diffusivities in the non-dimensional form D^i/D^∞ in Table 4. The particle diffusivity is estimated after the linear Stokes–Einstein regime is attained in the directional mean-squared-displacements (MSD^i). All D^i/D^∞ values decrease with blockage B (i.e. going downwards along the columns of Table 4), whereas the corresponding difference between the centerline and the off-axis positions at the same B is characterized by an increase in co-axial motion but a decrease in wall-normal motion (looking sideways along the rows of Table 4). This enhancement along the co-axial direction is also listed in Table 4. The hydrodynamic basis for this observed counter-intuitive trend is explained in terms of particle mobility enhancement below using the steady-state *CFD* framework.

5.2. Mobility enhancement in the co-axial direction

The noted anisotropy in the diffusive behavior is explained using the directional reduction in mobility, λ^i, of a non-Brownian spherical particle moving under similar conditions (a quiescent fluid). The reduction is deduced from the steady-state *CFD* simulations using Eq. (13). Owing to the theoretical relationship between D^i and λ^i (as shown in Eq. (9)),

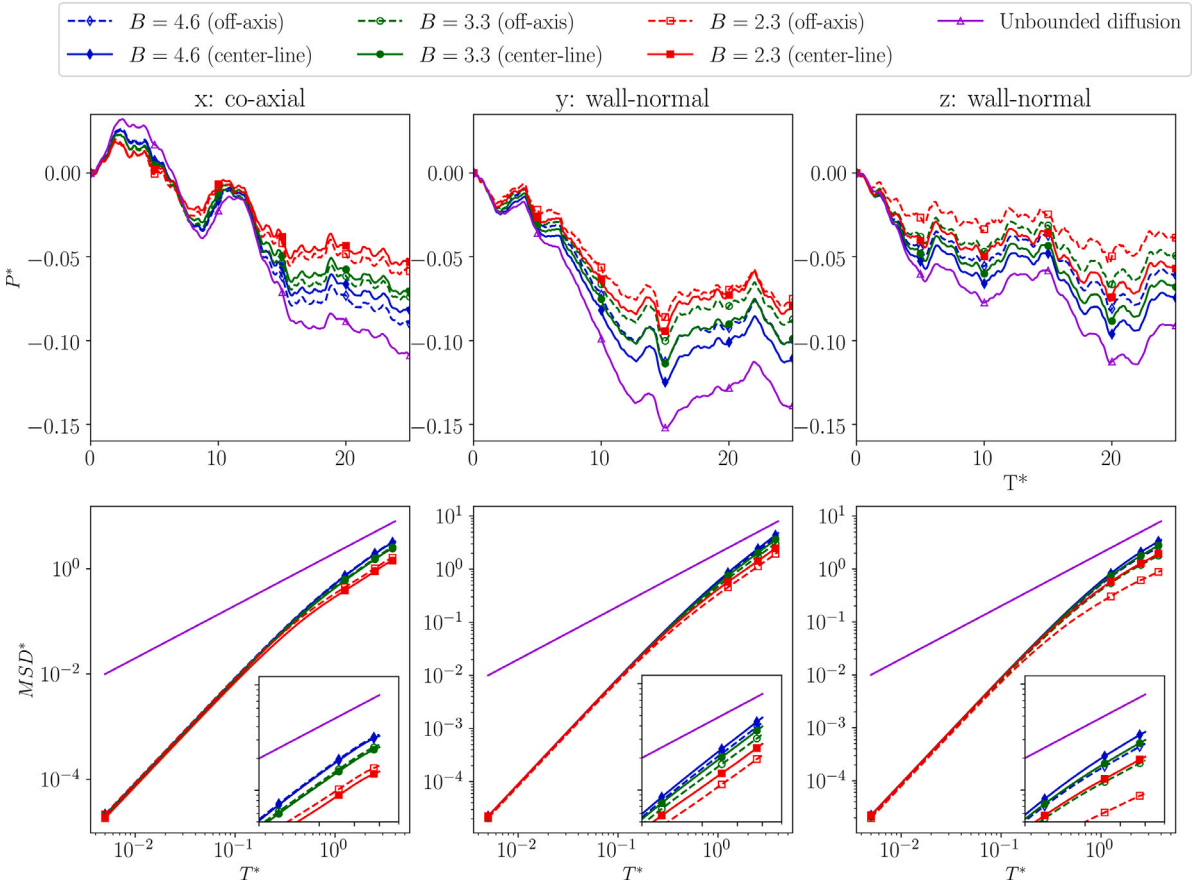

Fig. 3. Comparison of the centerline and off-axis hindered diffusion for a 400 nm Brownian particle under varying degrees of confinement (represented as the blockage ratios (B) 4.6, 3.3 and 2.3, respectively) along the co-axial (x) and wall-normal (z) directions. **Top panel**: the mean non-dimensional drift/displacement of the particle from the origin (estimated as $P^{i*} = p^{i*} - p^{i*}_{origin}$) over a 25 τ_p period. **Bottom panel**: the non-dimensional directional MSD^{i*} evaluated over $5\tau_p$ for a $100\tau_p$ period of motion. The purple solid lines (——) represent the analytical non-dimensionalized Stokes–Einstein behavior for unbounded Brownian motion (Eq. (9)). The insets show the linear diffusive regimes attained individually along each of these directions. Note the transition from a ballistic ($slope = 2$) to a linear diffusive regime. All reported drifts are calculated using the same random number sequence (**G**).

Table 4
Anisotropy in the non-dimensional directional diffusivities of a 400 nm Brownian particle in the x (co-axial) and z (wall-normal) directions after $5\tau_p$. Predictions of D^i/D_∞ from *LaIBM* are compared with $1/\lambda^i_{CFD}$, which is the mobility reduction deduced from steady-state *CFD* simulations (non-Brownian). Notice the enhanced diffusivity (due to lower mobility reduction) along the co-axial direction for the off-axis cases (at $a/4$) in both scenarios. The results listed in this table are of the same order of magnitude as those of Uma et al. (2011), Gentile et al. (2015) and Gubbiotti et al. (2019), that performed similar assessments.

Blockage ratio	Centerline				Off-axis				% enhancement	
	x_{LaIBM}	x_{CFD}	z_{LaIBM}	z_{CFD}	x_{LaIBM}	x_{CFD}	z_{LaIBM}	z_{CFD}	x_{LaIBM}	x_{CFD}
4.6	0.638	0.605	0.690	0.653	0.655	0.609	0.522	0.518	2.66%	0.72%
3.3	0.496	0.467	0.576	0.528	0.513	0.478	0.359	0.355	1.95%	2.34%
2.3	0.304	0.293	0.399	0.365	0.324	0.298	0.172	0.122	6.17%	1.76%

D_∞ is estimated from the corresponding unbounded Brownian diffusion simulations ($\lambda = 1$).

the expected effect on the diffusivity (in the diffusion simulations) of the Brownian particle can be directly estimated as:

$$\frac{D^i}{D^\infty} = \frac{1}{\lambda^i_{CFD}}. \tag{17}$$

Note that Eq. (17) is used to estimate the mobility reduction listed in Table 4. We emphasize that the *CFD* results are valid at the off-axis location $a/4$ exactly, while the *LaIBM* results represent an averaged behavior in the vicinity of this location due to the continuous motion of the particle. We also note that this effect on the local diffusivity as determined by *LaIBM* may vary with location in the channel, as the spatial variation of the particle mobility is not uniform. To provide a broader illustration of these mobility enhancement effects (along the co-axial direction) from the *CFD* simulations, we also list the maximum enhancement found and the corresponding location of these maxima (in terms of X^*) in Table 5. In general, it is clear that a relatively minor displacement towards the centerline from the off-axis location (at $a/4$) results in a noticeable increase in the enhancement of the co-axial diffusivity, which may at least partly explain why the *LaIBM* results (which depict a Brownian particle under continuous motion) are higher than the corresponding *CFD* results (which depict a non-Brownian particle) for two out of three blockage ratios in Table 4. Moreover, as the diffusing particle in *LaIBM* is sampling the variations in the particle mobility field in a region surrounding its initial location, the influence of these variations on the estimated diffusivity will vary with B. We furthermore stress that Table 5 does not necessarily reflect the global maxima, but only the maximum enhancement found in the locations probed in the *CFD* simulations.

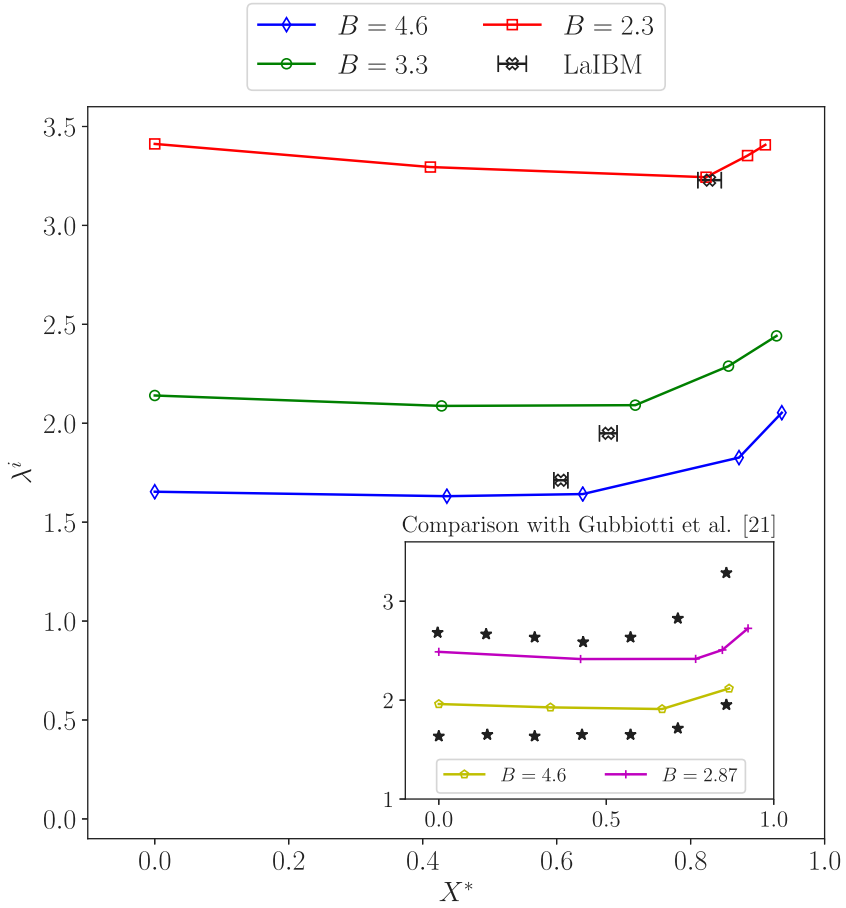

Fig. 4. Directional reduction in mobility, λ^i, along the co-axial direction at the blockage ratios (B) 4.6, 3.3 and 2.3, respectively, for the *CFD* simulations in a square micro-channel. Here, X^* is the non-dimensional z-location of the particle between the center of the channel and the walls. The inset shows the comparison between the DPD data of Gubbiotti et al. (2019) and our steady state *CFD* results in a cylindrical channel. Also plotted are the mean λ^i, extracted from the particle mean-squared behavior in the *LaIBM* framework with an error bar indicating the span of X^* visited by the particle in the simulation. Note the minimum in λ^i as the particle is shifted off-axis.

Table 5
Maximum % enhancements in the co-axial mobility and their corresponding positions when moving from a position on the centerline to an off-center position as obtained from the steady-state *CFD* analyses.

Blockage ratio	% enhancement	X^*_{max}
4.60	1.38%	0.436
3.30	2.52%	0.428
2.87	2.92%	0.423
2.30	5.19%	0.823

Overall we find that, as B decreases (i.e. the degree of confinement increases), the corresponding λ^i along the co-axial direction reduces to a minimum value as the particle is shifted off-axis, before increasing again. This trend in λ^i is plotted in Fig. 4. We also note that the existence of a minimum is in agreement with the data presented by Gubbiotti et al. (2019) (see Table 5 and the inset in Fig. 4). The noted enhancement along the co-axial direction is small enough to possibly be due to numerical uncertainties, however there could also be a hydrodynamic basis for the observed behavior. A strong argument for the latter hypothesis is that this trend is noticeable in both our *LaIBM* and steady-state *CFD* results for the square duct, as well as in the DPD results of Gubbiotti et al. (2019) and our steady-state *CFD* results for a cylindrical duct — i.e. that the effect is observed in three independent frameworks and in two different geometries. Moreover, as this phenomenon is absent in the limits of $B \to \infty$ (point particle) and $B \to 0$ (particle touching the walls), it is also clear that it can only exist in some range of intermediate values of B, thus making it more difficult to observe by chance. Furthermore, since a Brownian particle does not remain at an exact location as in the steady state (non-Brownian) simulations, slight differences in the particle mobility are expected. Despite these differences, the underlying hydrodynamic basis is still reflected in a continuum multiphase DNS approach (such as the *LaIBM*) as the hydrodynamic fields around the particle are resolved to a reasonable degree of accuracy. Correspondingly, the mean λ^i, extracted from the particle mean-squared behavior as the inverse of the values listed in Table 4, is plotted in Fig. 4 as well (with an error bar indicating the span of X^* visited by the particle). This comparison further confirms that the obtained particle mobilities are in agreement with the established hydrodynamic bases (under the period of observation). Furthermore, the steady-state *CFD* results are more closer to the analytical solution of Haberman and Sayre (1958) than the DPD results of Gubbiotti et al. (2019) (as shown in Table 2), which may be due to that the DPD approach exhibits a finite slip even at no-slip walls. Despite these differences, the appearance of the minima in both the results of Gubbiotti et al. (2019) and our steady *CFD* simulations, increases the plausibility of the described hydrodynamic basis.

Furthermore, it can be noted in Table 4 that the wall-normal diffusivity is somewhat overpredicted with *LaIBM* in comparison to the *CFD* results, particularly at the lowest value of B. A sphere traveling parallel to a wall may experience a lateral force attempting to move the particle either towards or away from the wall (Cox and Hsu, 1977; Takemura, 2004). In the simulations performed here, the Reynolds number is small and these effects are therefore also small: in the steady *CFD* simulations, the lateral force is three to four orders of magnitude smaller than the force in the direction of motion of the particle when the particle is moving parallel to the wall. Experiments on particles settling parallel

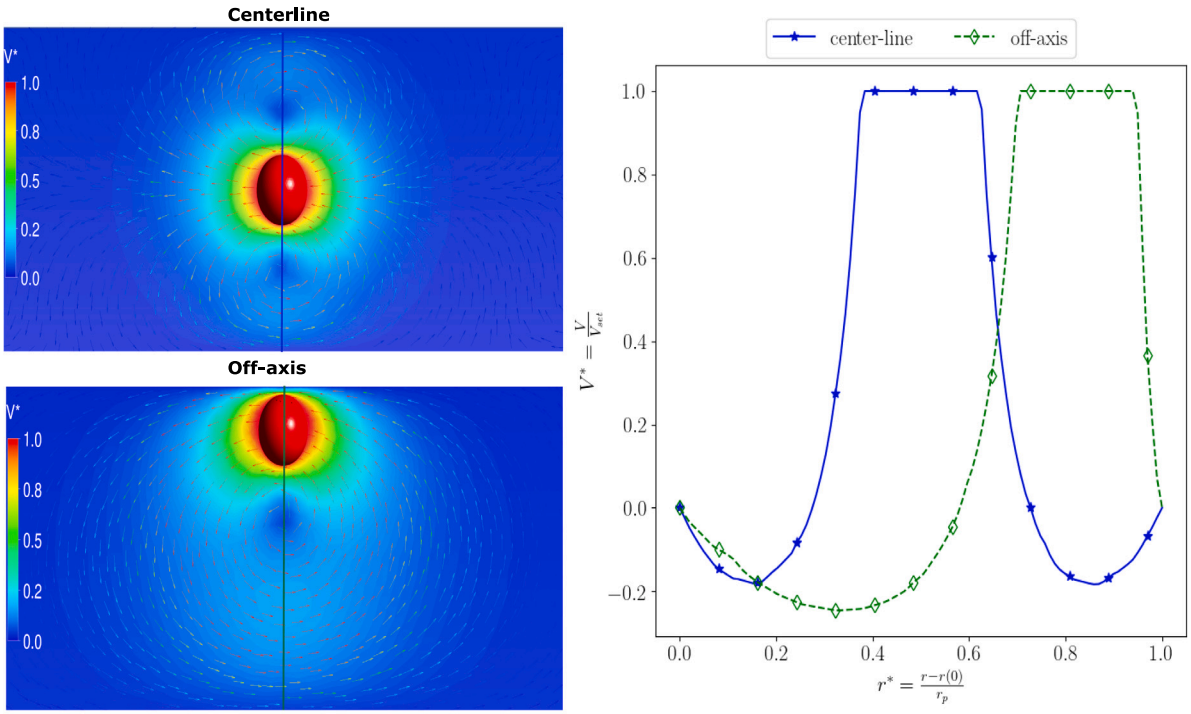

Fig. 5. Left panel: Re-circulation zones around a particle located at centerline and off-center positions. Contours of normalized co-axial fluid velocity ($V^* = \frac{V}{V_p}$) overlaid with flow vectors along the same direction (from the steady-state *CFD* simulations) in an x–z plane at $6.5d_p < x < 13.5d_p$ (i.e. a 6 d_p co-axial span around the particle), $y = w/2$ and $0 < z < a$. This normalization is done for a simplified visualization of the hydrodynamic zones. **Right panel**: V^* over a line passing through the center of the particle (i.e. $x = l/2$, $y = w/2$ and $0 < z < a$) plotted as a function of the non-dimensional distance $r^* = \frac{r-r(0)}{r_p}$ ($r^* = 0$ and $r^* = 1$ represent the location of the walls along the z-direction) at $B = 4.6$. Note the lack of a flow reversal in the region between the particle and the wall in the off-axis configuration.

to walls at Re = 0.18 show that the lateral migration velocity is less than 1% of the sedimentation velocity (Takemura, 2004). However, as *LaIBM* fully resolves the flow around the particles, the effects of lateral forces are inherently accounted for. Since the effect of lateral migration would be most pronounced at the lowest value of B, it is possible that a part of the discrepancy observed in Table 4 could be due to lateral forces.

5.3. A hydrodynamic basis for the anisotropy

In the limit of high values of B (not shown in this paper), the particle is small in relation to the duct and interacts with the walls only in its closest proximity. It is in this situation that λ^i is a monotonous function of the particle–wall distance, with the wall-normal interactions dominant over corresponding co-axial ones (as shown by Brenner (1961)). However, as the confinement becomes more pronounced, the walls around the entire duct perimeter start to influence the flow field around the particle, implying that friction along all wall-bounded sides contribute to the overall λ^i. More specifically, the co-axial motion of the particle necessitates that the fluid in its path is displaced in a recirculating motion where it fills the region between the particle and the confining walls due to continuity (see Fig. 5). These flows are symmetric on the centerline and asymmetric for off-axis positions.

The cross-sectional area available for the displaced fluid to pass the particle is independent of the particle position (in relation to the walls closest to it), but the resistance to this flow varies with the geometrical configuration. As the particle comes in close proximity to the wall, there is no longer room for a re-circulation pattern to develop in the narrow slit between the particle and the wall. The flow field asymmetry is therefore significantly enhanced as the flow reversal between the particle and the wall dies out and the sphere, instead, drags along the fluid in this narrow region. This lack of flow-reversal in between the particle and the wall is evident in the right panel of Fig. 5, which shows the normalized co-axial fluid velocity over a line passing a through the center of the particle across a centerline and off-axis motion at $B = 4.6$. Moving the particle off the centerline towards a wall increases the effective hydraulic diameter of the cross-section available for the flow without affecting the total flow rate, thus contributing to a lowering of the overall resistance. At the same time, the velocity gradient at the particle surface in the region between the particle and the wall goes to infinity as the particle–wall distance reduces, eventually causing a steep increase in the hydrodynamic resistance associated with the co-axial motion at small particle–wall separations. However, before that, the change of direction in the fluid motion within the narrow slit between the particle and the wall gives rise to the noticed minimum in λ^i.

Further, as B decreases, the particle fills up a larger portion of the channel cross-section and thus creates a relatively larger fluid displacement as it moves, leading to an increase in the overall hydrodynamic resistance. An increase in the effective hydraulic diameter, as obtained by moving the particle away from the centerline, therefore becomes more influential on the resistance, while at the same time shifting the location of minimal co-axial resistance further towards the wall as B decreases (see Fig. 4). The wall-normal motion, on the other hand, does not exhibit such a fundamental change of regimes, as the fluid in the region between the particle and the wall always has to be squeezed out irrespective of the wall–particle distance. Thus, these trends in the hydrodynamic resistances are responsible for the unexpected increase in co-axial diffusivity noted in the off-axis hindered diffusion of the Brownian particle.

This possibility for the existence of a minimum in the spatially varying friction can perhaps be even better understood by qualitative analysis of a simplified problem, as illustrated in Fig. 6. Here, we visualize the Stokes flow solutions to two similar flow problems formulated for the geometry of a square duct, intersected by a cylinder that is aligned with the main flow direction. The flow is either driven by a pressure gradient or by imposing a constant velocity on the cylinder wall. We then observe the different solutions depending on whether the cylinder is situated on the centerline or placed eccentrically. In

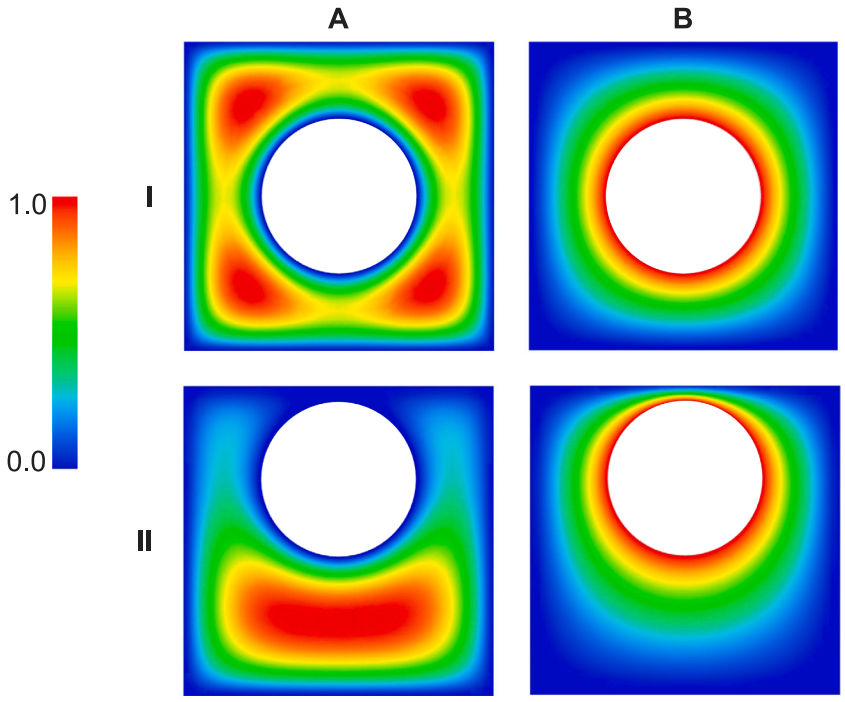

Fig. 6. Stokes flow solutions for fully developed flow in a square duct with a cylinder inside at $B = 2$. Column A: pressure-driven flow. Column B: drag-induced flow. Row I: cylinder placed on the centerline. Row II: cylinder placed eccentrically. The contours depict velocity magnitude in a plane perpendicular to the main flow direction, normalized by the maximum velocity. In this example, the force on the cylinder is higher in A-I than in A-II for the same pressure gradient, whereas it is higher in B-II than in B-I for the same velocity.

line with the above discussion for our case with the spherical particle, we observe that for the drag-induced flow cases (column B in Fig. 6), the force on the cylinder *increases* as the cylinder is brought closer to the wall. Conversely, the force on the cylinder *decreases* for the pressure-driven flow cases (column A in Fig. 6) when the cylinder is put closer to the wall. Moreover, the increase is more significant for the drag-induced flow cases than the decrease is for the pressure-driven cases. The explanation for this observation lies in the fact that once the cylinder is placed far enough away from the centerline in the pressure-driven flow, moving it further away has little influence — the main part of the flow already goes through the larger unaffected region below. For the drag-induced flow, however, the cylinder must always drag along the flow in between itself and the nearest wall, leading to an extreme increase in the required force at small cylinder-wall separation.

As the Stokes equations are linear, it is possible to add different solutions together to obtain new solutions to the same equations. More specifically, a linear combination of the pressure-driven and drag-induced flows will resemble the flow observed over the line passing through the center of the spherical particle in Fig. 5. It then follows naturally that such a linear combination of opposing mechanisms (of either increasing or decreasing the force on the particle as it is placed closer to the wall), together with the fact that these mechanisms differ in their dependence on the radial position of the particle, is enough to explain the appearance of a minimum in the force at some intermediate off-axis position. In other words, it is the backflow of fluid created by the motion of the particle that produces this minimum.

5.4. Implications for simulations of Brownian motion at intermediate confinements

The existence of an enhancement effect on the Brownian motion (of a spherical particle in a micro-channel) at intermediate confinements has several important implications for simulations of such phenomena at varying levels of abstraction. For example, the application of wall corrections to the hydrodynamics in non-interface resolving methods must be done with great care, as these are generally derived in the $B \rightarrow \infty$ limit where enhancement effects are not present. It is also still an open question as to how this enhancement effect may change due to the presence of other Brownian particles or in a pressure-driven flow through the channel. Further, one must expect that the delicate balance between hydrodynamic effects, thermal fluctuations and additional external fields not accounted for here (e.g. van der Waals-interactions or electrostatic double-layer interactions) can be very sensitive to the exact geometrical configuration in the near-wall region of narrow channels, indicating that failure to correctly account for the true hydrodynamic environment around the Brownian particle will lead to erroneous predictions of the extent of particle–wall interaction. Such facets are very relevant in several reactive or biological systems. In conclusion, these facts point to the importance of probing Brownian motion at intermediate confinements with a numerical simulation model that can leverage the local hydrodynamic environment *on-the-fly* to dictate the ensuing diffusion.

6. Conclusions

In this paper, we evaluate the off-axis diffusion of a spherical Brownian particle in a square micro-channel, under intermediate hydrodynamic confinements (i.e. the particle size is non-negligible in relation to the channel size while still not touching the walls). We show that, under these conditions, the co-axial diffusivity of a particle diffusing off-axis may be enhanced when compared with a corresponding centerline diffusion. This effect is augmented as the particle confinement increases. We attribute this increased particle diffusivity to a reduced co-axial fluid resistance when the particle is displaced off-center, through a hydrodynamic basis derived using steady-state *CFD* simulations of a spherical particle moving in a channel. More specifically, the direction of fluid motion in the narrow region between the particle and the wall changes with the particle–wall distance at low blockages B (where $B = a/d_p$, a is the side of the duct and d_p is the particle diameter), creating a position of minimum hydrodynamic resistance for co-axial motion at an off-axis location (which

in turn is a function of B). Such a minimum was noted in both our coupled continuum mechanics-Langevin multiphase DNS ($LaIBM$) and steady-state *CFD* results, as well as in the results reported in literature (the dissipative particle dynamics (DPD) results of Gubbiotti et al. (2019)). Thus, the noted enhancement along the co-axial direction for off-axis hindered diffusion – although small enough to blend-in with numerical uncertainties at a coarser resolution – does seem to have a firm hydrodynamic basis. Consequently, we demonstrate how the $LaIBM$ framework, which incorporates the instantaneous hydrodynamics into the Langevin equation of motion, can be used to probe such anisotropies in hindered diffusion phenomena. These inferences open up new avenues for advanced functional material design, where the complex influence of nano-structured system boundaries on the Brownian behavior of nanoparticles can be probed and optimized *in silico*. A large number of applications in rapidly emerging nano-engineering fields would significantly benefit from such capabilities.

CRediT authorship contribution statement

Ananda Subramani Kannan: Conceptualization, Methodology, Software, Validation, Formal analysis, Investigation, Data curation, Writing – original draft, Writing – review and editing. **Andreas Mark:** Methodology, Writing – Review and editing, Supervision. **Dario Maggiolo:** Methodology, Writing – Review and editing, Supervision. **Gaetano Sardina:** Methodology, Writing – Review and editing, Supervision. **Srdjan Sasic:** Conceptualization, Methodology, Writing – review and editing, Supervision. **Henrik Ström:** Conceptualization, Methodology, Software, Validation, Formal analysis, Writing – review and editing, Funding acquisition, Supervision.

Declaration of competing interest

The authors declare that they have no known competing financial interests or personal relationships that could have appeared to influence the work reported in this paper.

Acknowledgments

The authors would like to thank the center for scientific and technical computing at Chalmers University of Technology (*C3SE*), for providing the necessary computational resources. This work has been financed by the Swedish Research Council (Vetenskapsrådet, Dnr 2015-04809).

Appendix A. Supplementary data

Supplementary material related to this article can be found online at https://doi.org/10.1016/j.ijmultiphaseflow.2021.103772.

References

Ayyaswamy, Portonovo S., Muzykantov, Vladimir, Eckmann, David M., Radhakrishnan, Ravi, 2013. Nanocarrier hydrodynamics and binding in targeted drug delivery: Challenges in numerical modeling and experimental validation. J. Nanotechnol. Eng. Med. (ISSN: 1949-2944) 4 (1), http://dx.doi.org/10.1115/1.4024004.

Batchelor, G.K., 1976. Brownian diffusion of particles with hydrodynamic interaction. J. Fluid Mech. 74 (1), 1–29. http://dx.doi.org/10.1017/S0022112076001663.

Bevan, Michael A., Prieve, Dennis C., 2000. Hindered diffusion of colloidal particles very near to a wall: revisited. J. Chem. Phys. (ISSN: 00219606) 113 (3), 1228–1236. http://dx.doi.org/10.1063/1.481900.

Brenner, Howard, 1961. The slow motion of a sphere through a viscous fluid towards a plane surface. Chem. Eng. Sci. (ISSN: 00092509) 16 (3–4), 242–251. http://dx.doi.org/10.1016/0009-2509(61)80035-3.

Brenner, H., 1982. A general theory of taylor dispersion phenomena IV. Direct coupling effects. Chem. Eng. Commun. 18 (5–6), 355–379. http://dx.doi.org/10.1080/00986448208939976.

Burada, P. Sekhar, Hänggi, Peter, Marchesoni, Fabio, Schmid, Gerhard, Talkner, Peter, 2009. Diffusion in confined geometries. ChemPhysChem (ISSN: 14397641) 10 (1), 45–54. http://dx.doi.org/10.1002/cphc.200800526, URL arXiv:0808.2345.

Chandrasekhar, S., 1943. Stochastic problems in physics and astronomy. Rev. Modern Phys. 15 (1), 1–89. http://dx.doi.org/10.1103/RevModPhys.15.1.

Choi, C.K., Margraves, C.H., Kihm, K.D., 2007. Examination of near-wall hindered Brownian diffusion of nanoparticles: Experimental comparison to theories by Brenner (1961) and Goldman et al. (1967). Phys. Fluids (ISSN: 10706631) 19 (10), http://dx.doi.org/10.1063/1.2798811.

Cox, R.G., Hsu, S.K., 1977. The lateral migration of solid particles in a laminar flow near a plane. Int. J. Multiph. Flow. (ISSN: 0301-9322) 3 (3), 201–222. http://dx.doi.org/10.1016/0301-9322(77)90001-5.

Dechadilok, Panadda, Deen, William M., 2006. Hindrance factors for diffusion and convection in pores. Ind. Eng. Chem. Res. 45 (21), 6953–6959. http://dx.doi.org/10.1021/ie051387n.

Deen, W.M., 1987. Hindered transport of large molecules in liquid-filled pores. AIChE Journal (ISSN: 15475905) 33 (9), 1409–1425. http://dx.doi.org/10.1002/aic.690330902.

Derks, Roy J.S., Frijns, Arjan J.H., Prins, Menno W.J., Dietzel, Andreas H., 2008. Self-organized twinning of actuated particles for microfluidic pumping. Appl. Phys. Lett. (ISSN: 00036951) 92 (2), http://dx.doi.org/10.1063/1.2834851.

Dufresne, Eric R., Squires, Todd M., Brenner, Michael P., Grier, David G., 2000. Hydrodynamic coupling of two brownian spheres to a planar surface. Phys. Rev. Lett. (ISSN: 00319007) 85 (15), 3317–3320. http://dx.doi.org/10.1103/PhysRevLett.85.3317.

Farago, Oded, Grønbech-Jensen, Niels, 2014. Langevin dynamics in inhomogeneous media: Re-examining the Itô-Stratonovich dilemma. Phys. Rev. E 89, 013301. http://dx.doi.org/10.1103/PhysRevE.89.013301.

Felderhof, B.U., 2005. Effect of the wall on the velocity autocorrelation function and long-time tail of Brownian motion. J. Phys. Chem. B (ISSN: 15206106) 109 (45), 21406–21412. http://dx.doi.org/10.1021/jp051335b.

Gentile, Francesco S., Santo, Ilaria De, D'Avino, Gaetano, Rossi, Lucio, Romeo, Giovanni, Greco, Francesco, Netti, Paolo A., Maffettone, Pier Luca, 2015. Hindered Brownian diffusion in a square-shaped geometry. J. Colloid Interface Sci. (ISSN: 10957103) 447, 25–32. http://dx.doi.org/10.1016/j.jcis.2015.01.055.

Göhl, Johan, Mark, Andreas, Sasic, Srdjan, Edelvik, Fredrik, 2018. An immersed boundary based dynamic contact angle framework for handling complex surfaces of mixed wettabilities. Int. J. Multiph. Flow. (ISSN: 0301-9322) http://dx.doi.org/10.1016/j.ijmultiphaseflow.2018.08.001.

Göhl, Johan, Markstedt, Kajsa, Mark, Andreas, Håkansson, Karl, Gatenholm, Paul, Edelvik, Fredrik, 2018. Simulations of 3D bioprinting: predicting bioprintability of nanofibrillar inks. Biofabrication 10 (3), 034105, URL http://stacks.iop.org/1758-5090/10/i=3/a=034105.

Grassia, P.S., Hinch, E.J., Nitsche, L.C., 1995. Computer simulations of Brownian motion of complex systems. J. Fluid Mech. 282, 373–403. http://dx.doi.org/10.1017/S0022112095000176.

Gubbiotti, Alberto, Chinappi, Mauro, Casciola, Carlo Massimo, 2019. Confinement effects on the dynamics of a rigid particle in a nanochannel. Phys. Rev. E 100, 053307. http://dx.doi.org/10.1103/PhysRevE.100.053307.

Haberman, W.L., Sayre, R.M., 1958. Motion of Rigid and Fluid Spheres in Stationary and Moving Liquids Inside Cylindrical Tubes. Technical report, Department of the navy - David Taylor model basin, URL http://hdl.handle.net/1721.3/48988.

Happel, John, Brenner, Howard, 1983. Low Reynolds Number Hydrodynamics. Martinus Nijhoff Publishers, http://dx.doi.org/10.1007/978-94-009-8352-6, ISBN: 13: 978-90-247-2877-0.

Higdon, J.J.L., Muldowney, G.P., 1995. Resistance functions for spherical particles, droplets and bubbles in cylindrical tubes. J. Fluid Mech. 298, 193–210. http://dx.doi.org/10.1017/S0022112095003272.

Ingelsten, Simon, Mark, Andreas, Edelvik, Fredrik, 2019. A Lagrangian–Eulerian framework for simulation of transient viscoelastic fluid flow. J. Non-Newton. Fluid Mech. (ISSN: 0377-0257) 266, 20–32. http://dx.doi.org/10.1016/j.jnnfm.2019.02.005.

Ingelsten, Simon, Mark, Andreas, Jareteg, Klas, Kádár, Roland, Edelvik, Fredrik, 2020. Computationally efficient viscoelastic flow simulation using a Lagrangian–Eulerian method and GPU-acceleration. J. Non-Newton. Fluid Mech. (ISSN: 0377-0257) 279, 104264. http://dx.doi.org/10.1016/j.jnnfm.2020.104264.

Itô, Kiyosi, 1973. Stochastic integration. In: Tucker, Don H., Maynard, Hugh B. (Eds.), Vector and Operator Valued Measures and Applications. Academic Press, ISBN: 978-0-12-702450-9, pp. 141–148. http://dx.doi.org/10.1016/B978-0-12-702450-9.50020-8.

Johnson, Tomas, Jakobsson, Stefan, Wettervik, Benjamin, Andersson, Björn, Mark, Andreas, Edelvik, Fredrik, 2015. A finite volume method for electrostatic three species negative corona discharge simulations with application to externally charged powder bells. J. Electrost. (ISSN: 0304-3886) 74, 27 – 36. http://dx.doi.org/10.1016/j.elstat.2014.12.009.

Kannan, Ananda Subramani, Mark, Andreas, Maggiolo, Dario, Sardina, Gaetano, Sasic, Srdjan, Ström, Henrik, 2021. Assessment of hindered diffusion in arbitrary geometries using a multiphase DNS framework. Chem. Eng. Sci. (ISSN: 0009-2509) 230, 116074. http://dx.doi.org/10.1016/j.ces.2020.116074.

Kannan, Ananda Subramani, Naserentin, Vasileios, Mark, Andreas, Maggiolo, Dario, Sardina, Gaetano, Sasic, Srdjan, Ström, Henrik, 2019. A continuum-based multiphase DNS method for studying the Brownian dynamics of soot particles in a rarefied gas. Chem. Eng. Sci. (ISSN: 0009-2509) 210, 115229. http://dx.doi.org/10.1016/j.ces.2019.115229.

Kihm, K.D., Banerjee, A., Choi, C.K., Takagi, T., 2004. Near-wall hindered Brownian diffusion of nanoparticles examined by three-dimensional ratiometric total internal reflection fluorescence microscopy (3-D R-TIRFM). Exp. Fluids (ISSN: 07234864) 37 (6), 811–824. http://dx.doi.org/10.1007/s00348-004-0865-4.

Kim, Sangtae, Karrila, Seppo J., 1991. Microhydrodynamics: Principles and Selected Applications. Butterworth-Heinemann, ISBN: 9781483161242.

Langevin, Paul, 1908. Sur la théorie du mouvement brownien. C. R. Acad. Sci. (Paris) 146, 530–533. http://dx.doi.org/10.1119/1.18725.

Lau, A.W.C., Lubensky, T.C., 2007. State-dependent diffusion: Thermodynamic consistency and its path integral formulation. Phys. Rev. E 76, 011123. http://dx.doi.org/10.1103/PhysRevE.76.011123.

Li, Amy, Ahmadi, Goodarz, 1992. Dispersion and deposition of spherical particles from point sources in a turbulent channel flow. Aerosol Sci. Technol. 16 (4), 209–226. http://dx.doi.org/10.1080/02786829208959550.

MacKay, G.D.M., Mason, S.G., 1961. Approach of a solid sphere to a rigid plane interface. J. Colloid Sci. (ISSN: 0095-8522) 16 (6), 632–635. http://dx.doi.org/10.1016/0095-8522(61)90049-6.

Mark, Andreas, Rundqvist, R., Edelvik, Fredrik, 2011. Comparison between different immersed boundary conditions for simulation of complex fluid flows. Fluid Dyn. Mater. Process. 7, 241–258. http://dx.doi.org/10.3970/fdmp.2011.007.241.

Mark, A., Svenning, E., Edelvik, F., 2013. An immersed boundary method for simulation of flow with heat transfer. Int. J. Heat Mass Transfer (ISSN: 0017-9310) 56 (1), 424–435. http://dx.doi.org/10.1016/j.ijheatmasstransfer.2012.09.010.

Mark, Andreas, van Wachem, Berend G.M., 2008. Derivation and validation of a novel implicit second-order accurate immersed boundary method. J. Comput. Phys. (ISSN: 0021-9991) 227 (13), 6660–6680. http://dx.doi.org/10.1016/j.jcp.2008.03.031.

Mavrovouniotis, Gretchen M., Brenner, Howard, 1988. Hindered sedimentation, diffusion, and dispersion coefficients for brownian spheres in circular cylindrical pores. J. Colloid Interface Sci. (ISSN: 00219797) 124 (1), 269–283. http://dx.doi.org/10.1016/0021-9797(88)90348-7.

Michaelides, Efstathios E., 2016. Wall effects on the Brownian movement, thermophoresis, and deposition of nanoparticles in liquids. J. Fluids Eng. (ISSN: 0098-2202) 138 (5), http://dx.doi.org/10.1115/1.4032030.

Mittal, Rajat, Iaccarino, Gianluca, 2005. Immersed boundary methods. Annu. Rev. Fluid Mech. 37 (1), 239–261. http://dx.doi.org/10.1146/annurev.fluid.37.061903.175743.

Mo, Jianyong, Raizen, Mark G., 2019. Highly resolved Brownian motion in space and in time. Annu. Rev. Fluid Mech. 51 (1), 403–428. http://dx.doi.org/10.1146/annurev-fluid-010518-040527.

Newmark, Nathan M., 1959. A method of computation for structural dynamics. J. Eng. Mech. Div. 85, 67–94.

Ounis, H., Ahmadi, G., 1990a. Analysis of dispersion of small spherical particles in a random velocity field. J. Fluids Eng. (ISSN: 0098-2202) 112 (1), 114–120. http://dx.doi.org/10.1115/1.2909358.

Ounis, Hadj, Ahmadi, Goodarz, 1990b. A comparison of Brownian and turbulent diffusion. Aerosol Sci. Technol. (ISSN: 0278-6826) 13 (1), 47–53. http://dx.doi.org/10.1080/02786829008959423.

Peskin, C.S., 1982. The fluid dynamics of heart valves: Experimental, theoretical, and computational methods. Annu. Rev. Fluid Mech. 14 (1), 235–259. http://dx.doi.org/10.1146/annurev.fl.14.010182.001315.

Radhakrishnan, Ravi, Farokhirad, Samaneh, Eckmann, David M., Ayyaswamy, Portonovo S., 2019. Chapter two - nanoparticle transport phenomena in confined flows. In: Sparrow, Ephraim M., Abraham, John P., Gorman, John M., Minkowycz, W.J. (Eds.), Advances in Heat Transfer. In: Advances in Heat Transfer, vol. 51, Elsevier, (ISSN: 0065-2717) pp. 55–129. http://dx.doi.org/10.1016/bs.aiht.2019.08.002.

Rundqvist, Robert, Mark, Andreas, Andersson, Björn, Ålund, Anders, Edelvik, Fredrik, Tafuri, Sebastian, Carlson, Johan S., 2010. Simulation of spray painting in automotive industry. In: Kreiss, Gunilla, Lötstedt, Per, Målqvist, Axel, Neytcheva, Maya (Eds.), Numerical Mathematics and Advanced Applications 2009. Springer Berlin Heidelberg, Berlin, Heidelberg, ISBN: 978-3-642-11795-4, pp. 771–779. http://dx.doi.org/10.1007/978-3-642-11795-4_83.

Skaug, Michael J., Wang, Liang, Ding, Yifu, Schwartz, Daniel K., 2015. Hindered nanoparticle diffusion and void accessibility in a three-dimensional porous medium. ACS Nano 9 (2), 2148–2156. http://dx.doi.org/10.1021/acsnano.5b00019.

Sokolov, Stanislav V., Kätelhön, Enno, Compton, Richard G., 2016. Near-wall hindered diffusion in convective systems: Transport limitations in colloidal and nanoparticulate systems. J. Phys. Chem. C (ISSN: 19327455) 120 (19), 10629–10640. http://dx.doi.org/10.1021/acs.jpcc.6b01640.

Squires, Todd M., Messinger, Robert J., Manalis, Scott R., 2008. Making it stick: Convection, reaction and diffusion in surface-based biosensors. Nature Biotechnol. (ISSN: 10870156) 26 (4), 417–426. http://dx.doi.org/10.1038/nbt1388.

Takemura, Fumio, 2004. Migration velocities of spherical solid particles near a vertical wall for Reynolds number from 0.1 to 5. Phys. Fluids 16 (1), 204–207. http://dx.doi.org/10.1063/1.1629129.

Uhlenbeck, G.E., Ornstein, L.S., 1930. On the theory of the Brownian motion. Phys. Rev. 36 (5), 823–841. http://dx.doi.org/10.1103/PhysRev.36.823.

Uma, B., Swaminathan, T.N., Radhakrishnan, R., Eckmann, D.M., Ayyaswamy, P.S., 2011. Nanoparticle Brownian motion and hydrodynamic interactions in the presence of flow fields. Phys. Fluids 23 (7), 073602. http://dx.doi.org/10.1063/1.3611026.

Versteeg, Henk Kaarle, Malalasekera, Weeratunge, 1995. An Introduction to Computational Fluid Dynamics - the Finite Volume Method. Addison-Wesley-Longman, ISBN: 978-0-582-21884-0, pp. I–X, 1–257.

Wettervik, Benjamin, Johnson, Tomas, Jakobsson, Stefan, Mark, Andreas, Edelvik, Fredrik, 2015. A domain decomposition method for three species modeling of multi-electrode negative corona discharge – with applications to electrostatic precipitators. J. Electrost. (ISSN: 0304-3886) 77, 139–146. http://dx.doi.org/10.1016/j.elstat.2015.08.004.